Electron-stimulated oxidation of Al(111) by oxygen at low temperatures: Mechanism of enhanced oxidation kinetics

V. Zhukov, I. Popova, and J. T. Yates, Jr.
Department of Chemistry, Surface Science Center, University of Pittsburgh, Pittsburgh, Pennsylvania 15260
(Received 26 December 2000; published 24 April 2002)

In this paper, the enhancement of the Al(111) oxidation rate by simultaneous oxygen exposures and electron irradiation is investigated at 90 K using X-ray photoelectron spectroscopy (XPS) and work-function (WF) measurements. Electron-beam energies of ~0–100 eV and current densities up to 80 μA/cm^2 are used. No effect of electron irradiation is found at the initial stages of oxidation. The effect (enhanced oxidation rate) is only observed at higher O_2 exposures (above 100 L), when clusters of aluminum oxide are formed on the surface. The existence of a molecular O_2 precursor state associated with these clusters is proposed, based on both the surface temperature and beam-energy dependence of the oxidation rate. In addition, charge trapped on the oxide grains sets up an electrostatic field (detected by XPS and WF measurements) stimulating ion diffusion and further oxide film growth.

DOI: 10.1103/PhysRevB.65.195409 PACS number(s): 34.80.Ht, 79.20.Hx, 79.60.Dp

I. INTRODUCTION

Electron-stimulated oxidation may lead to fast and controllable growth of insulating oxide films.[1–3] Various aspects of the effect of electron irradiation on surface processes, such as, electron-stimulated desorption,[4] diffusion,[5] and dissociative electron attachment[6,7] (DEA) have been already discussed in the literature. There is no accepted generalized theory of electron-stimulated oxidation, most likely due to the high specificity of the oxidation process to the system being studied, demanding, in each case, individual consideration.

Electron-stimulated oxidation of various semiconductor surfaces has been carried out,[1–3,8(a,b)] showing the enhancement of the otherwise low rate of oxidation by the simultaneous presence of the electron beam and adsorbed water or oxygen molecules. Electron-stimulated oxidation of Si by oxygen was carefully studied, showing a resonance in the dependence of the oxidation rate on the primary beam energy, which corresponded to the onset of the lowest DEA transition.[3] Electron attachment to an adsorbed O_2 precursor molecule with the formation of a temporary negative ion and subsequent dissociation were therefore proposed for the mechanism of electron-stimulated oxidation.[3]

The use of electron beams to stimulate metal oxidation is also an important topic. It has been investigated for a number of metals, such as, Cu, Ni (both–O_2+electrons), Al (H_2O +electrons), etc.[9–11] Detailed studies of Ni(111) oxidation have been performed at various temperatures, suggesting the operation of a different mechanism for oxidation with and without the electron beam.[10] In the initial stages of Ni(111) oxidation, the presence of the electron beam did not influence the oxidation kinetics. Electron irradiation was postulated to produce defect sites at the later stages of oxidation, which enhance the oxidation process. This conclusion was drawn from the fact that oxygen exposures following electron irradiation resulted in the production of the same total oxygen coverage as exposures carried out simultaneously with electron irradiation.

The Al(111) surface is known to exhibit a low sticking coefficient at 300 K for oxygen adsorption (5×10^{-3},5×10^{-2},2×10^{-2}).[12–14(a)] Numerous studies have pointed to the strong nonadiabaticity and steric limitations of the O_2 adsorption process.[13,15] The presence of a molecular precursor state on the surface prior to O_2 dissociation was previously postulated, based on the observed temperature dependence of the sticking coefficient.[14(a)] It was also shown that electron irradiation stimulates the transformation of chemisorbed O species on the surface to oxidic species.[16] Enhanced Al(111) oxidation kinetics were observed for simultaneous exposure to water and electrons (100 eV, 20 μA/cm^2) as detected by X-ray photoelectron spectroscopy[11] (XPS). Linear oxide growth kinetics were observed during electron irradiation, in contrast to the parabolic rate law observed for thermal oxidation. This effect was ascribed to the production of the temporary negative ion H_2O^-, which decomposes with the formation of an OH radical, a strong oxidizing agent. In addition, the presence of a constant electric field across the film during the electron-assisted process was proposed to explain the linear oxide growth kinetics.[11]

Numerous studies of the work-function change of the Al(111) surface upon oxygen adsorption have been performed in the past.[17(a)–(e)] A decrease in the surface work function upon oxygen exposure was reported (ranging from -0.15 to -0.4 eV at the maximum work-function change upon oxidation). Relatively small values of the work-function change (and associated with them surface dipole moment) were observed despite the strong electron transfer between adsorbate and Al atoms, and were associated with the small adsorption distances for the O species.[17(a)] Despite inconsistencies in the values, observed by different groups,[17(b)–(e)] a single model involving oxygen adsorption on top and O incorporation into the Al-metal layer was used to describe the experimental results.[17(c)] The presence of incorporated (subsurface) oxygen species, a postulate based on the work-function decrease, has dominated thinking about Al oxidation in the last 10–15 yr.[17(b)]

In this study we explore the oxide growth mechanism on Al(111) in the presence of an electron beam. Coupling our spectroscopic methods with work-function measurements

 ©2002 The American Physical Society

allows us to correlate changes in the electrostatic surface potential in the process of oxidation with the electron-stimulated oxidation rate. We correlate the electron energy threshold in the oxidation rate with dissociative electron attachment to O_2, leading to enhanced oxidation.

II. EXPERIMENTAL METHODS

The studies were conducted in a UHV chamber [$(2-3)\times 10^{-10}$ Torr base pressure] equipped with XPS, Auger electron spectroscopy, other standard analytical methods, and a rastering electron gun, setup for sample irradiation and work-function (WF) measurements. Details of the mounting and cleaning procedures for the Al(111) crystal may be found in Ref. 14(b). The surface structure and its cleanliness were checked with low-energy electron diffraction and XPS prior to all experiments.

The mechanism of the electron-stimulated oxidation with oxygen was investigated in the surface temperature range of 90–300 K (measured by a type-K thermocouple). Oxygen gas (Matheson Co., 99.999% pure) was dosed into a separate reaction chamber, isolated from the rest of the system (exposure up to 3000 L, $1\ \mathrm{L}=1\times 10^{-6}$ Torr s) through a leak valve by back-filling up to 1×10^{-7} Torr pressure (uncorrected for the ion gauge sensitivity).

A rastering electron gun was used as a source of electrons (beam diameter ~0.5 mm) with the primary energy in the range of 0–200 eV and with current densities of up to 20 μA/cm^2. At this current density the electron interaction with O_2 molecules in the gaseous phase is negligible. During adsorption experiments the focused electron beam is scanned across the crystal surface. The gun setup involves synchronization of the beam rastering with a video monitor, allowing visualization of the treated surface area by imaging the crystal in the secondary electron-emission mode. A retarding field was applied, allowing us to decrease the electron energy to near ~0 eV (without beam defocusing). Measurements in both the fixed primary current (variable energy) and fixed primary beam-energy (variable primary current) modes were performed.

In the experimental setup described above, the interaction time of the electron beam with a particular point at the surface was only 4×10^{-8} s (based on the beam diameter and rastering frequencies). To check whether the effects observed here are related to the fast rastering rate of the electron beam, the measurements were also performed with the broad-beam electron gun (100–200 eV) with a current density in the 10–80 μA/cm^2 range. In this way, we found that the absence of the effect of the electron beam on the oxidation kinetics during the initial stages cannot be attributed to the short lifetime of the surface oxygen species.

The oxygen coverage resulting from simultaneous oxygen exposures and electron bombardment was measured using XPS. The thickness of the oxide layer was estimated using relative attenuation of the metallic $Al^0(2p)$ XPS peak in the process of oxide growth,[18] taking into account the electron attenuation length (16.7 ± 0.6 Å).[19] The measurements of the $O(1s)$ intensity were correlated with the oxide thickness measurements based on the attenuation of the metallic $Al^0(2p)$ XPS peak.

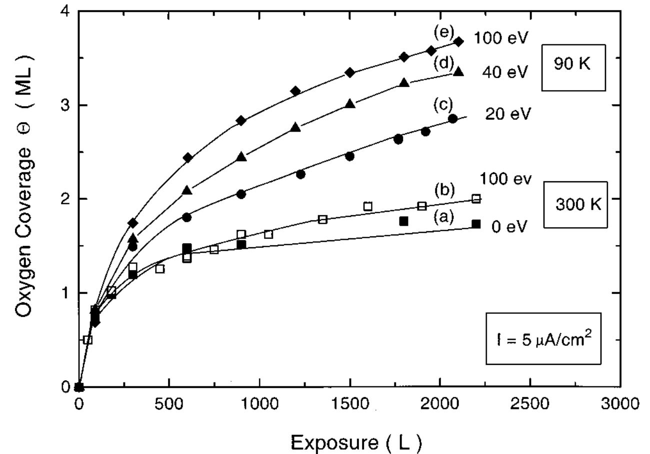

FIG. 1. Uptake curves for oxygen adsorption both with and without simultaneous electron irradiation are shown. (a) thermal oxidation at 300 K, (b) with 100 eV electrons at 300 K, (c) 20 eV at 90 K, (d) 40 eV at 90 K, (e) 100 eV at 90 K. An electron current density of 5 μA/cm^2 was used for all the measurements.

Changes in the secondary electron-emission yield were recorded in the process of electron-stimulated oxidation for various electron energies. For this, the primary current I_p (in the emitter circuit) and collected current I_c (in the sample circuit) were measured for each exposure. The value of the secondary electron yield (SEY) was established as $Y_{\mathrm{SE}}=(I_p-I_c)/I_p$ (ratio of the secondary and primary currents).

The surface work function was measured by recording I-V curves with the electron gun running in the retarding field mode, using the standard method for measuring the surface potential changes during adsorption, typically described as the "thermionic-diode" method. The measured values (energy position of the midpoint of the I-V curve in the oxidation process) were then referenced to the work function of the clean Al(111) (4.2 eV Ref. 20) to obtain the magnitude of the absolute work function during oxidation. Details of this procedure can be found in Ref. 21.

III. RESULTS

The oxygen-uptake curves (expressed as oxide film thickness) for electron-assisted oxidation of Al(111) were recorded for various electron beam energies and sample currents. No effect of electron irradiation on the initial sticking coefficient [exposures below 100 L Ref. 14(a)] was found for surface temperatures in the 90–300 K range and up to 500 eV beam energy ($I=20\ \mu$A/cm^2). An enhanced oxidation rate in the presence of electrons was observed at higher O_2 exposures. Figure 1 shows representative oxygen-uptake curves for oxidation without electrons (open symbols) and with electrons for a current density of 5 μA/cm^2, and beam energies of 0–100 eV (solid symbols).

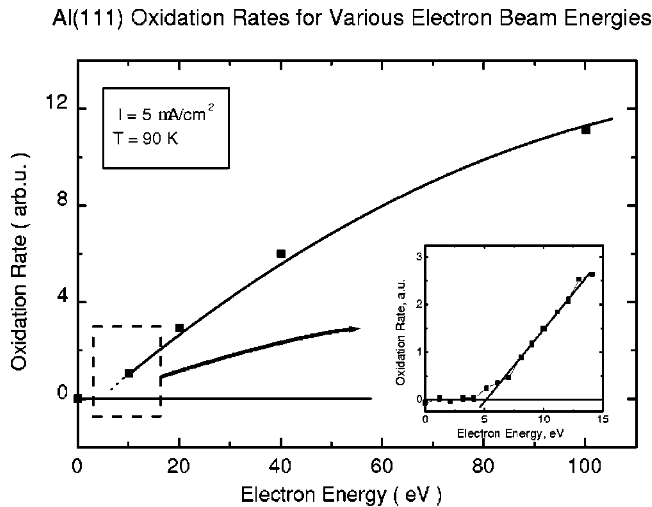

FIG. 2. Dependence of the electron-stimulated oxidation rate (at $T=90$ K) on the beam energy. Inset—low energy regime (0–15 eV). The measurements are taken in the retarding field mode.

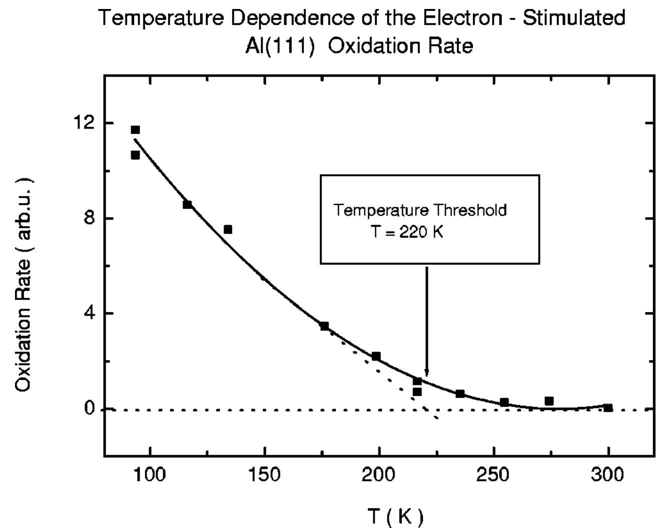

FIG. 3. Temperature dependence of the electron-stimulated oxidation rate ($E_p=100$ eV,$I=5$ μA/cm^2). A temperature threshold near 220 K is observed.

At 300 K, the use of electrons of various energies (up to 500 eV) during O_2 exposure was observed to influence the uptake rate slightly only above exposures of ~1500 L [curves (*a*) and (*b*) in Fig. 1]. The uptake curves for oxidation at 90 K demonstrating increasing oxidation rate with higher electron beam energy are also shown in Fig. 1 [curves (*c*), (*d*), and (*e*) for 20, 40, and 100 eV, respectively]. These experiments show a significant effect of electron irradiation on enhancing the oxidation kinetics above an O_2 exposure of ~100 L.

The oxidation rate under electron stimulation was defined at 90 K as $R=(d\theta/d\,\exp)_{\mathrm{with\ electrons}}-(d\theta/d\,\exp)_{\mathrm{w/o\ electrons}}$ and calculated at the same total oxygen coverage ($\theta_O \approx 2$ ML) for various beam energies. The rate of electron-assisted oxidation was found to depend linearly on the beam current density for electron beam energies in the 10–200 eV range. The energy dependence of the oxidation rate for 5 μA/cm^2 current density is shown in Fig. 2. Separate experiments were made to detect the low-energy threshold for the electron-assisted oxidation under the surface conditions where the electron-stimulated oxidation effect is large. For this, a thermally grown oxide layer (1200 L O_2 exposure) was further oxidized by oxygen and electrons of variable beam energy. The threshold in the oxidation was observed for beam energies near 5 eV (corrected for cathode work function) as shown in the inset in Fig. 2.

To determine the effect of surface temperature, the oxidation rate was measured for exposures above 1200 L ($\theta_O \geqslant 1.5$ ML) at progressively lower temperatures (Fig. 3). A temperature threshold for electron-assisted oxidation is observed near 220 K. The increase in the adsorption rate with decreasing surface temperature indicates the involvement of an O_2 precursor state on top of the oxide layer (see Sec. IV).

We investigated the correlation between the secondary electron-emission yield of the surface in the process of electron-stimulated oxidation at 90 K for various electron energies. Figure 4 shows measured secondary electron yield as a function of the oxygen exposure for $E_p=20$ (circles), 40 (triangles), and 100 eV (diamonds). As may be seen, essentially similar behavior is seen for the electron energies shown (gradual increase of SEY upon oxidation), consistent with the gradual transformation of the oxidized layer from a conducting film to an insulating film.

Two patterns of the work-function behavior in the course of oxidation were observed (Fig. 5). The work-function variation is displayed vs oxygen coverage (the coverage calibration was performed using uptake curves from Fig. 1). In the case of thermal oxidation, the work function decreased monotonically for increasing oxide coverage (Fig. 5, circles). The maximum observed work-function decrease is 0.6 eV. In contrast, for the electron-assisted oxidation, the work-function decrease (minimum at 0.9 eV at $\theta=0.75$ ML, corresponding to 100 L O_2 exposure) is followed by an increase, reaching a work function higher than for the clean surface by 0.4 eV as shown in Fig. 5 (squares). These measurements are

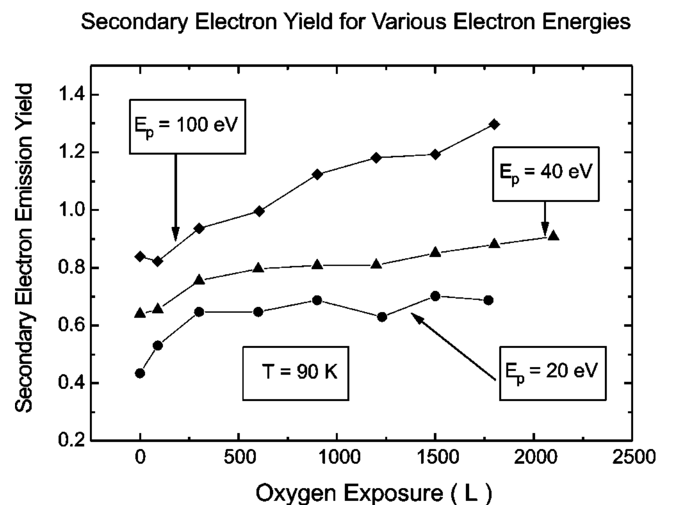

FIG. 4. Changes of the secondary emission yield (SEY) in the process of electron-assisted oxidation at 90 K for $E_p=20$ (circles), 40 (triangles), and 100 eV (diamonds). The monotonic increase of SEY observed for different beam energies is consistent with the transformation of the substrate into the insulating oxide film.

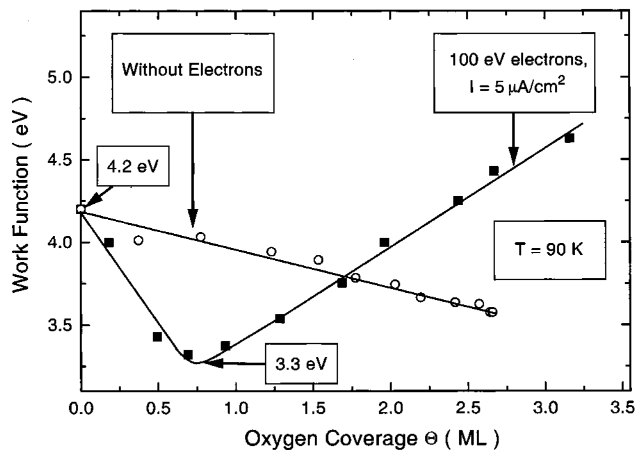

FIG. 5. Work-function changes observed for oxidation at 90 K are shown as a function of the total oxygen coverage: circles—oxidation by O_2 gas without an electron beam; squares—with 100 eV electrons ($I = 5\ \mu A/cm^2$). Measurements were made using 5×10^{-10} A current. The coverage calibration is based on the uptake curves from Fig. 1. The reversal in the slope of the work-function change (with electron beam, squares) at 0.75 ML coverage ($\varepsilon = 100$ L) corresponds to the beginning of formation of oxide particles on the surface.

consistent with the enhancement of oxidation kinetics by electron bombardment.

IV. DISCUSSION

A. Initial stages of oxidation

No changes in the adsorption kinetics were introduced by the presence of the electron beam in the initial stages of oxidation (exposures below 100 L, $T = 90-300$ K, electron energies up to 500 eV). Precursor-mediated O_2 adsorption, found earlier on Al(111), needs to be considered to explain this result.[14(a)] The lack of a significant influence of the electron beam on the oxidation rate at low-O_2 exposures may be explained in several ways.

(1) The interaction of the electron beam with the precursor O_2 molecule on the surface is negligible, possibly limited by the available flux of electrons (0.2 e/s per surface atom) or by the short lifetime of the precursor on the surface at low oxygen coverages.

(2) The effect of electron-stimulated dissociation of the O_2 precursor, enhancing the oxidation rate is canceled by the electron-stimulated desorption of O_2 precursor, giving a net zero (or even slightly negative) effect.

(3) The interaction of the electron beam with the precursor O_2 molecule significantly enhances the oxidation kinetics only after the oxide clusters have formed on the surface (100 L exposure of O_2).

Experiments using higher electron current densities delivered from a flood gun (up to 80 $\mu A/cm^2$ corresponding to ~ 0.5 e/s per surface atom) did not result in an increase of the observed oxidation rate, suggesting that electron flux may not be the limiting factor.

B. Electron-stimulated oxidation

For O_2 exposures above ~ 100 L at 90 K, a strong enhancement of the oxidation rate is observed in the presence of the electron beam. Our previous high-resolution electron-energy-loss study of Al(111) oxidation at 300 K demonstrated that the distribution of the adsorbing O species between the chemisorbed and oxidic surface phases is influenced by electron irradiation.[16] Unlike unassisted oxidation, where oxide formation was negligible below 300 L,[14b] in the presence of the electron beam oxidation was observed at lower O_2 exposures due to the electron-stimulated transformation of the chemisorbed O to oxidic species.[16] Thus, for exposures above 100 L, the presence of oxide grains on the surface is postulated for the electron-assisted process.

1. Role of the molecular O_2 precursor in the electron-assisted oxidation

We have observed a temperature threshold for the electron-stimulated oxidation rate at 220 K, suggesting the involvement of the molecular O_2 precursor state on the surface (Fig. 3). As the temperature is lowered, the coverage and lifetime of the O_2 precursor will increase under the steady-state conditions. The presence of this state on top of the oxide layer was previously postulated by ultraviolet photoelectron spectroscopy studies.[22] An analysis of our oxidation rate data[23] in the Arrhenius fashion indicated a nonactivated process, with a difference of desorption and adsorption energies $(E_d - E_a) \approx (80 \pm 8)$ meV for the molecular precursor. This type of analysis of the adsorption data was previously used and described in detail in Ref. 14(a).

Additional evidence for the proposed precursor state on the surface comes from the proximity of the observed electron-energy threshold (5 ± 1 eV, Fig. 2 inset) to the threshold value observed for the onset of the cross section for dissociative electron attachment to the gas-phase O_2 molecule (~ 4.4 eV at 300 K).[24] A resonance in the dissociative attachment cross section observed around 6.7 eV was ascribed to the formation of the single compound O_2^- state $X\ ^2\Pi_u$. Decay of the temporary negative-ion states may proceed through autoionization, with the formation of excited O_2 molecules, or through dissociation with the formation of the excited O and O^- states.[24] All of the possible species are more reactive than ground-state O_2 molecules.

Both the temperature and the energy dependence of the oxidation rate are only observed for O_2 exposures above 100 L, suggesting that the molecular precursor state is correlated with the formation of oxide grains. They can stabilize the precursor state itself or the temporary negative ions, formed as a result of the electron attachment process to the O_2 molecule. The lifetime of these ion states is likely to increase on top of the insulating oxide grains, which will prevent loss of the negative charge.

2. Charge storage on the oxide grains and its influence on the oxidation rate

During the electron irradiation, in addition to dissociative attachment to the precursor molecule (as discussed above), electrons can also create an electric charge on the oxide grains. The presence of an electric field across the oxide in the process of electron-assisted oxidation was indicated by the rigid shift of both Al($2p$) and O($1s$) oxidic peaks to

lower binding energy and by changes in the work function (see the following section) in the oxidation process. XPS core level Al($2p$) and O($1s$) oxidic peaks shift rigidly (up to 1 eV) in the direction opposite to the one observed during the thermal oxidation of Al.[14(a)] Both techniques suggest negative charging of the growing oxide layer.

Possible mechanisms of the effect of the electrostatic field across the growing oxide film involve partial electron transfer at earlier stages of the molecule's approach to the charged surface (i.e., at higher molecule-surface distances) and subsequent participation of the oxide clusters in the dissociation of the adsorbed molecules. The role of charge storage on the oxide clusters on the kinetics of oxidation will be investigated in the future.[25]

A number of stable shallow potential well O_2^- states was proposed to exist at the high internuclear O-O separation,[24] which may result from the electron transfer from the charged oxide grains to the antibonding O_2 molecular orbitals, leading to the weakening of the O-O bond. For example, the compound O_2^- state ($X\ ^2\Pi_g$) formed by electron attachment at low energies ($E_p = 0-1$ eV) ($v = 0-3$) is reported to lie below the ground state of O_2 on the potential-energy diagram.[24] This result supports the model proposed here with electron transfer occuring from the charged oxide grains to the precursor O_2 molecule on the surface.

3. Enhanced oxidation rate in the presence of the electric field

The presence of stable charge on the surface of oxide particles results in the formation of an electric field across the particle. This field is postulated to play an important role in the process of the metal oxidation, according to the Cabrera-Mott theory.[26(a)] Electron tunneling from the metal into the broadened and lowered affinity levels of the adsorbate creates an excess negative charge on the outer part of the growing oxide film.[26(a)] In the coupled current modification of this theory,[26(b)] the balance of electronic (electrons tunneling from the metal) and ionic (cation and anion) current creates an electrostatic potential across the oxide film. The field stimulates ion diffusion—the rate-limiting step of the thermal oxide-growth process. The oxide growth stops at the limiting oxide film thickness, when the value of the field in each of the unit cells is lower than the corresponding barrier for ion diffusion.[26(a,b)] In the case of electron-stimulated oxidation, the presence of the electrostatic potential [up to the breakdown voltage of bulk alumina [$(3-13) \times 10^6$ V/cm] Ref. 27], constantly replenished by the electron beam, removes this limitation and results in the oxidation kinetics with no saturation of the oxide-growth rate (up to exposures of 2000–3000 L in this study). (Both cations and anions are participating in the mass transport in the process of Al oxide growth, since mobilities of oxygen and aluminum ions are roughly comparable).[26(a)] Similar results were obtained for electron-stimulated Al(111) oxidation with H_2O.[11] This conclusion correlates with the dependence of the oxidation rate on the electron current density, where higher current density produces a larger electrostatic field across the growing layer, inducing a higher oxidation rate.

4. Possible role of the secondary electrons in the electronic excitation process

A comparison of Fig. 4 to Fig. 1 demonstrates the absence of a correlation between the oxidation rate and the secondary electron-emission coefficient in the course of the oxide layer growth. The changes in the secondary electron-emission coefficient are consistent with the transformation of the substrate from conductive to insulating material (higher value for a thicker oxide layer) for all investigated electron beam energies.

Figure 2 (inset) shows an electron-energy threshold for electron-stimulated oxidation phenomena at 5 ± 1 eV. In the range of 5–15 eV, a monotonic increase in the oxidation rate occurs. For the various electron attachment processes to the O_2 molecule, a resonance at low electron energies,[24] with a falloff of excitation rate above the resonance energy is observed. In contrast, we observed a monotonic dependence on the electron energy (Figure 2, inset). This behavior may be a consequence of the production of the secondary electrons exhibiting a broad energy spectrum and obscuring or even eliminating the observation of a peak resonance electron energy.

C. Work-function changes upon O_2 adsorption

We observe that for the unassisted Al(111) oxidation at 90 K the work function decreases linearly by 0.22 eV for a surface O coverage of 1 ML (Fig. 5, circles). In contrast, when oxidation was carried out in the presence of the electron beam (100 eV, 5 μA), the initial decrease of the work function was followed (after exposure of 100 L) by an *increase* of 0.4 eV above the value for the clean surface.

For adsorption of the electronegative oxygen species on Al, the decreasing work function was previously interpreted as being due to the production of a subsurface O species.[17] In

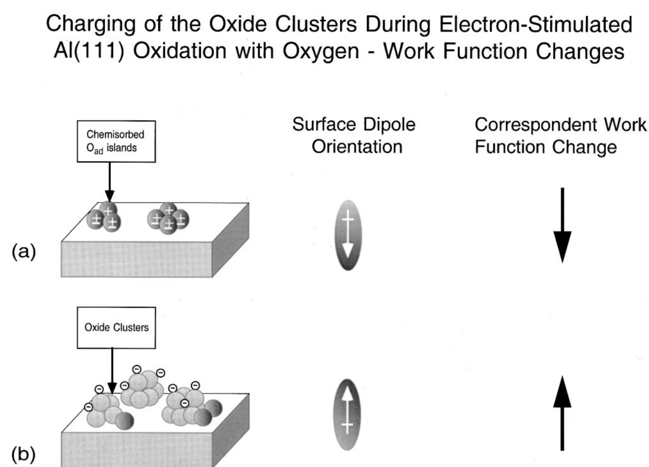

FIG. 6. Schematic diagram illustrating the changes in the surface work function with the dipole orientation: (a) only chemisorbed oxygen is present, giving a positive outward dipole orientation and a decrease of the work function; (b) lower panel - charging of the oxide grains reverses the dipole orientation, causing an increase of the work function.

contrast, scanning-tunnel-microscope (STM) studies[12] indicate that subsurface oxygen does not exist during adsorption of O_2 on Al(111) at 300 K. The sign of the work-function change upon adsorption (without the electron beam) is rather caused by charge redistribution between the surface atoms and adsorbate and depends on the type of bonding formed (chemisorbed or oxidic).

The initial decrease of the work function (observed both for oxidation with and without simultaneous electron irradiation) is associated with the polarization of the absorbed species, creating a net positive outward dipole. Once formed, oxide grains (above ~100 L exposure) may be negatively charged by the electron beam. This reverses the overall dipole orientation (Fig. 6, lower panel), causing an increase of the work function [linearly with the surface coverage (Fig. 5)]. The appearance of the oxide grains (~100 L O_2 exposure) and the development of the negative electrostatic potential on the surface correlates with the increase in the electron-assisted oxidation rate. The electrostatic potential further promotes additional oxidation by stimulating ion diffusion, as postulated in the Cabrera-Mott theory of metal oxidation.[26] The electric field is kept constant by the supply of electrons. Thus the film thickness increases monotonically when the electrons are incident on the growing oxide film, whereas in unassisted oxidation, saturation occurs, causing ion diffusion to stop.

V. CONCLUSIONS

The rate of the electron-stimulated oxidation of Al(111) using oxygen gas was investigated at 90 K for electron energies of ~0–100 eV and current densities up to 80 $\mu A/cm^2$. The following conclusions were made.

(1) The enhancement of the electron-stimulated oxidation rate of Al(111) by O_2 results from a combination of two different effects.

(a) The formation of a temporary negative O_2^- ion by an electron attachment to the molecular oxygen precursor, dissociating into the reactive O species and leading to enhanced oxidation kinetics.

(b) The charging of the outer surface of the oxide grains producing on electric field across the grains, promoting the ionic and electronic transport in the process of oxide film growth and leading to increased oxidation rate.

(2) An energy threshold to the dissociative electron attachment to the precursor O_2 molecule is observed around 5 eV, consistent with electron attachment to O_2.

(3) The O_2 precursor electron-assisted dissociation, producing an enhanced oxidation rate, is observed only in the presence of the oxide grains on the surface.

ACKNOWLEDGMENT

We thank the Air Force Office of Scientific Research for support for this work.

[1] M. C. Muñoz and J. L. Sacedón, J. Chem. Phys. **74**, 4693 (1981).
[2] H. Schade, Appl. Surf. Sci. **24**, 1270 (1985).
[3] J. Xu, W. J. Choyke, and J. T. Yates, Jr., J. Appl. Phys. **82**, 6289 (1997).
[4] R. Ramsier and J. T. Yates, Jr., Surf. Sci. Rep. **12**, 243 (1991).
[5] A. G. Fedorus, E. V. Klimenko, A. G. Naumovets, E. M. Zasimovich, and I. N. Zasimovich, Nucl. Instrum. Methods Phys. Res. B **101**, 207 (1995).
[6] L. Sanche, J. Phys. B **23**, 1597 (1990).
[7] J. W. Gadzuk, Surf. Sci. **342**, 345 (1995).
[8] (a) Y. Sugimoto, M. Taneya, K. Akita, and H. Kawanishi, J. Appl. Phys. **69**, 2725 (1991); (b) C. Webb, J. Lagowski, and M. Lichteinsteiger, Surf. Sci. **138**, 399 (1984).
[9] J. M. Heras and L. Viscido, J. Vac. Sci. Technol. A **15**, 2051 (1997).
[10] (a) W. Li, M. J. Stirniman, and S. J. Sibener, Surf. Sci. **329**, L593 (1995); (b) W. Li, M. J. Stirniman, S. J. Sibener, J. Vac. Sci. Technol. A **13**, 1574 (1995).
[11] (a) H. D. Ebinger and J. T. Yates, Jr., Phys. Rev. B **57**, 1976 (1998); (b) Surf. Sci. **412/413**, 1 (1998)
[12] H. Brune, J. Wintterlin, J. Trost, G. Ertl, J. Wiechers, and R. J. Behm, J. Chem. Phys. **99**, 2128 (1993).
[13] B. Kasemo, E. Törnqvist, J. K. Norskov, and B. I. Lundqvist, Surf. Sci. **89**, 554 (1979).
[14] (a) V. Zhukov, I. Popova, and J. T. Yates, Jr., Surf. Sci. **441**, 251 (1999); (b) V. Zhukov, I. Popova, V. Fomenko, and J. T. Yates, Jr., *ibid.* **441**, 240 (1999).
[15] Y. Yourdshahyan, Ph.D. thesis, Department of Applied Physics, Chalmers University of Technology, Göteborg, 1999.
[16] I. Popova, V. Zhukov, and J. T. Yates, Jr., Appl. Phys. Lett. **75**, 3108 (1999).
[17] (a) N. D. Lang, Surf. Sci. **127**, L118 (1983); (b) V. K. Agarwala and T. Fort, Jr., *ibid.* **45**, 470 (1974); (c) R. L. Wells and T. Fort, Jr., *ibid.* **33**, 172 (1972); (d) P. O. Gartland, *ibid.* **62**, 183 (1977); (e) R. Michael, J. Gastaldi, C. Allasia, C. Jourdon, and J. Derrien, *ibid.* **95**, 309 (1980).
[18] H. Graupner, L. Hammer, K. Heinz, and D. M. Zehner, Surf. Sci. **380**, 335 (1997).
[19] D. R. Penn, J. Electron. Spectrosc. Rel Phenom. **9**, 29 (1976).
[20] *CRC Handbook of Chemistry and Physics*, 71st ed., edited by D. R. Lide (CRC Press, Boca Raton, FL, 1990).
[21] T. P. Ershova, S. G. Ershov, V. E. Zhukov, V. V. Korablev, and V. Y. Tyukin, Fiz. Tekhn. Poluprovodn. **23**, 323 (1989) [Sov. Phys. Semicond. **23**, 199 (1989)].
[22] P. Hofmann, W. Wyrobisch, and A. M. Bradshaw, Surf. Sci. **80**, 344 (1979).
[23] The slopes of the uptake curves from Fig. 1 were evaluated at constant coverage to calculate the relative values of the adsorption rates for different electron energies. An Arrhenius analysis of the obtained values yielded (80 ± 8) meV as a difference of desorption and adsorption activation energies.
[24] G. J. Schulz, Rev. Mod. Phys. **45**, 423 (1973).
[25] I. Popova, V. Zhukov, and J. T. Yates, Jr. (unpublished).
[26] (a) F. P. Fehlner and N. F. Mott, Oxid. Met. **2**, 59 (1970); (b) A. T. Fromhold, Jr., *Theory of Oxidation*, Defects in Crystalline Solids Vol. 1 (North-Holland, Amsterdam, 1976).
[27] N. Klein and M. Albert, J. Appl. Phys. **53**, 5840 (1982).